POLITECNICO DI TORINO
Repository ISTITUZIONALE

Efficiency Mapping of Electrically Excited Synchronous Motors with Different Control Strategies

Original
Efficiency Mapping of Electrically Excited Synchronous Motors with Different Control Strategies / Graffeo, F., Rubino, S., Jimenez Molina, M.S., Vaschetto, S., Tenconi, A.. - (2025), pp. 1-6. (2025 IEEE Workshop on Electrical Machines Design, Control and Diagnosis (WEMDCD) Malta 9-10 April 2025) [10.1109/wemdcd61816.2025.11014137].

Availability:
This version is available at: 11583/3001101 since: 2025-06-18T15:50:43Z

Publisher:
IEEE

Published
DOI:10.1109/wemdcd61816.2025.11014137

Terms of use:

This article is made available under terms and conditions as specified in the corresponding bibliographic description in the repository

Publisher copyright
IEEE postprint/Author's Accepted Manuscript

©2025 IEEE. Personal use of this material is permitted. Permission from IEEE must be obtained for all other uses, in any current or future media, including reprinting/republishing this material for advertising or promotional purposes, creating new collecting works, for resale or lists, or reuse of any copyrighted component of this work in other works.

(Article begins on next page)

18 October 2026

Efficiency Mapping of Electrically Excited Synchronous Motors with Different Control Strategies

Federica Graffeo
Dipartimento Energia
Politecnico di Torino
Torino, Italy
federica.graffeo@polito.it

Sandro Rubino
Dipartimento Energia
Politecnico di Torino
Torino, Italy
sandro.rubino@polito.it

Matías Jiménez Molina
Dipartimento Energia
Politecnico di Torino
Torino, Italy
matias.jimenez@polito.it

Silvio Vaschetto
Dipartimento Energia
Politecnico di Torino
Torino, Italy
silvio.vaschetto@polito.it

Alberto Tenconi
Dipartimento Energia
Politecnico di Torino
Torino, Italy
alberto.tenconi@polito.it

***Abstract*—Electrically excited synchronous motors (EESMs) have gained significant attention in the transportation sector due to their ability to eliminate the need for rare-earth materials. One critical tool for evaluating and optimizing the performance of EESMs is the efficiency mapping, which provides insights into the motor's behavior across a wide range of operating conditions. This paper presents a comprehensive methodology for generating efficiency maps of EESMs based on the machine flux and loss maps, readily obtainable through finite element simulations or direct prototype measurements. Additionally, the proposed methodology accounts for multiple control strategies enabled by the three degrees of freedom offered by the rotor current and the stator *d*- and *q*-axis currents. Indeed, while traditional approaches focus on minimizing total losses to optimize overall efficiency, alternative strategies - such as reducing rotor losses, maximizing power factor, or minimizing *d*-axis current - can offer targeted advantages, including improved thermal management and optimized inverter design. To demonstrate the effectiveness of this approach, an electric motor equipping a commercially available vehicle is used as a case study, with efficiency maps computed for five distinct control strategies. The findings highlight the adaptability of EESMs to meet different performance requirements, making them a versatile solution for electrified powertrains.**

***Index Terms*—efficiency mapping, electrically excited, wound field, synchronous motors**

I. Introduction

Electrically Excited Synchronous Motors (EESMs), also known as wound-field synchronous motors, have attracted increasing attention across various applications due to their inherent flexibility in controlling the excitation field [1], [2]. This flexibility allows EESMs to deliver high torque at low speeds without overloading the stator windings, as well as maintaining constant power operation across a theoretically unlimited speed range [3]. Unlike permanent magnet synchronous machines, EESMs utilize a controllable field excitation provided by a wound rotor, enabling precise adaptation to diverse operating conditions. Thanks to the rotor winding, EESMs eliminate the reliance on rare-earth materials, thereby addressing both environmental sustainability and supply-chain concerns associated with permanent magnets [4].

In recent years, the focus on energy efficiency and sustainable development has driven significant interest in optimizing electric machines' performance. Among the key challenges is the accurate characterization of the motor's efficiency across its operational envelope. Efficiency mapping serves as a critical tool for this purpose, providing insights into loss distribution and enabling the development of advanced control strategies aimed at minimizing energy consumption. Efficiency maps are particularly significant in applications requiring operation across multiple points on the torque-speed plane, such as in traction systems. In these scenarios, the motor operates at various load and speed conditions, where energy losses play a crucial role in determining the overall battery range.

The computation of efficiency maps for electric machines has been extensively studied in the literature [5], [6]. However, the majority of these works are focused on permanent magnet machines. These approaches are inadequate for electrically excited synchronous motors, as they do not account for the additional degree of freedom introduced by the rotor current, which significantly impacts the efficiency map computation.

Existing studies on EESMs are relatively sparse, and those available typically focus on the traditional objective of minimizing total losses [7]–[9]. While effective for maximizing efficiency, this approach does not fully leverage the unique control flexibility of EESMs. Indeed, alternative control strategies can be tailored to specific goals. For example, minimizing rotor losses can improve thermal performance, maximizing power factor can enhance inverter efficiency.

In this context, this paper proposes a methodology for the efficiency mapping of electrically excited synchronous motors,

This study was carried out within the MOST – Sustainable Mobility National Research Center and received funding from the European Union Next-GenerationEU (PIANO NAZIONALE DI RIPRESA E RESILIENZA (PNRR) – MISSIONE 4 COMPONENTE 2, INVESTIMENTO 1.4 – D.D. 1033 17/06/2022, CN00000023). This manuscript reflects only the authors' views and opinions, neither the European Union nor the European Commission can be considered responsible for them.

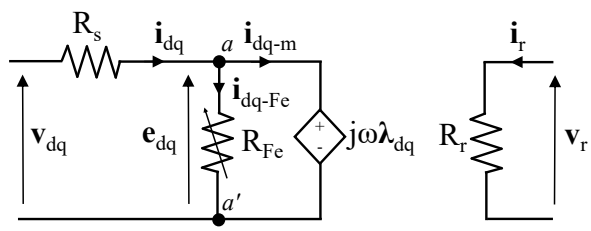

Fig. 1. Steady-state equivalent circuit.

based on the machine flux and loss maps that can be easily obtained through finite element (FE) simulations or direct measurements on a motor prototype. The proposed approach allows for easy adaptation of the efficiency maps to drivetrain constraints, such as maximum voltage, current, speed, and torque limits, as well as considering different temperature conditions. Moreover, the procedure is designed to consider various control strategies, enabling a detailed assessment of how different strategies influence the overall motor efficiency.

The ability to off-line recompute efficiency maps under varying operating conditions represents a key advantage of this methodology. Indeed, conducting tests across multiple conditions can be both time-consuming and resource-intensive. On the other hand, in the absence of a prototype, the proposed approach relies entirely on finite element simulations to generate the necessary data, offering a practical and flexible solution for efficiency assessment during the machine design stage.

To demonstrate the applicability of the proposed methodology, efficiency maps are generated using the developed algorithm for an automotive traction motor from an actual production vehicle, considering five different control strategies.

II. Electrically Excited Machine Model

The proposed efficiency mapping procedure is based on the electromagnetic model of the EESM defined in the rotating *dq* reference frame, where the *d*-axis is aligned to the magnetic field produced by the rotor winding. The *dq* equivalent circuit of EESM in steady-state conditions is shown in Fig. 1.

The voltage equations for the considered equivalent circuit, expressed in complex notation, are:

$$\begin{cases} \mathbf{v}_{dq} = R_s \cdot \mathbf{i}_{dq} + \mathbf{j} \cdot \omega_e \cdot \boldsymbol{\lambda}_{dq} \\ v_r = R_r \cdot i_r \end{cases} \tag{1}$$

In (1), $\mathbf{v}_{dq} = v_d + \mathbf{j} \cdot v_q$ represents the stator voltage, $\mathbf{i}_{dq} = i_d + \mathbf{j} \cdot i_q$ is the stator current, and $\boldsymbol{\lambda}_{dq} = \lambda_d + \mathbf{j} \cdot \lambda_q$ denotes the stator flux linkage. Additionally, v_r and i_r refer to the rotor voltage and current, while R_s and R_r are the stator and rotor resistances, and ω_e is the electrical angular frequency.

In the equivalent circuit, the flux linkages λ_d and λ_q depend on the current $\mathbf{i}_{dq-m}$. In this paper, the flux linkages are represented as Look-Up Tables (LUTs), defined as functions of (i_{d-m}, i_{q-m}, i_r), as shown in (2).

$$\begin{cases} \lambda_d = f_d(i_{d-m}, i_{q-m}, i_r) \\ \lambda_q = f_q(i_{d-m}, i_{q-m}, i_r) \\ \lambda_r = f_r(i_{d-m}, i_{q-m}, i_r) \end{cases} \tag{2}$$

These LUTs can be generated using FE simulations or by conducting direct measurements on the motor [10]. In the efficiency mapping computation, the LUTs are used to interpolate the flux linkages for any given combination of the currents i_{d-m}, i_{q-m}, and i_r.

For what concerns the resistor R_{Fe}, its losses correspond to the machine's iron losses, which depend on the current $\mathbf{i}_{dq-m}$. Similar to the flux linkages, LUTs are derived for the stator and rotor iron losses. In this paper, the iron losses are computed through FE by directly processing the field solution for each mesh element, as detailed in [5]. The calculation is based on the Steinmetz equation for specific core losses (W/kg):

$$p_{Fe,0} = k_h \cdot f_0^{\alpha} \cdot B^{\beta} + k_e \cdot (f_0 \cdot B)^2 \tag{3}$$

In (3), the frequency f_0 is the operating frequency at which the losses are evaluated, and B is the magnetic flux density. The first term represents the specific hysteresis losses, while the second corresponds to specific eddy current losses. The coefficients k_h, k_e, α, and β can be determined by fitting the measured loss curve of the core material. The computed losses must be stored in LUTs, distinguishing between hysteresis and eddy current losses. Differentiating between stator and rotor losses is only necessary when using two different materials for the stator and rotor cores or when stator or rotor losses are the target of the control strategy.

The stator and rotor resistances R_s and R_r can be determined either through analytical estimations or direct measurements on the prototype. These values are necessary for the machine copper losses computation. In this work, the mechanical and AC copper losses have been neglected.

Finally, the flux maps enable the calculation of the motor's electromagnetic torque for any given combination of phase currents, as:

$$T_m = \frac{3}{2} \cdot p \cdot (\lambda_d \cdot i_q - \lambda_q \cdot i_d) \tag{4}$$

III. Efficiency Mapping Algorithm

The efficiency mapping algorithm evaluates the motor's performance across a range of torque (T_m) and speed (n_m) values. The core logic of the algorithm involves iteratively calculating feasible operating points, determining associated losses, and identifying optimal conditions based on the chosen control strategy objective. The flowchart for the efficiency mapping is depicted in Fig. 2, where i is the index of the loop variable and N_t is the size of the efficiency map matrix.

A. Maps Initialization and IsoTorque Computation

The algorithm begins by initializing the torque-speed map as a grid of discrete torque values (T_m) and speed values (n_m):

$$T_m \in [T_{\min}, T_{\max}], \quad n_m \in [n_{\min}, n_{\max}]. \tag{5}$$

For each torque level (T_m), the flux maps described in (2) are used to generate iso-torque data. This involves identifying all possible combinations of $i_{d\text{-}m}$, $i_{q\text{-}m}$, and i_r current components that can produce the specified torque. In this paper, the identification is performed in Matlab environment using '*isosurface*' command on upscaled flux maps.

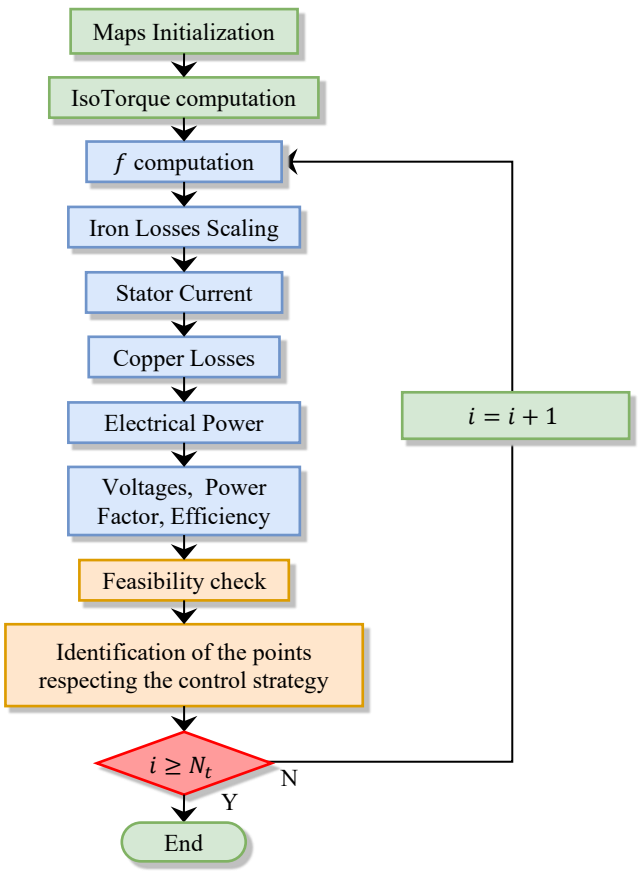

Fig. 2. Efficiency Mapping Algorithm Flowchart.

B. Computations on the (T_m, n_m) Plane

For each torque value, the following computations are then applied to each combination of current components.

1) Frequency and Back-EMF Computation: at each operating point defined by (T_m, n_m), the electrical frequency f is calculated, considering the machine pole pairs p. Using the calculated frequency, the back-EMF voltages are determined:

$$e_d = -\omega_e \cdot \lambda_q, \quad e_q = \omega_e \cdot \lambda_d, \quad e_{dq} = \sqrt{e_d^2 + e_q^2} \tag{6}$$

2) Iron Losses Scaling: the iron losses are obtained by scaling the FE computed iron losses with the operating frequency:

$$P_{Fe} = P_{\text{h},0} \cdot \left(\frac{f}{f_0}\right)^{\alpha} + P_{\text{e},0} \cdot \left(\frac{f}{f_0}\right)^{2} \tag{7}$$

where P_{Fe} is the sum of the stator and rotor iron losses, $P_{Fe,s}$ and $P_{Fe,r}$, for the considered frequency. On the other hand, $P_{\text{h},0}$ is the sum of the stator and rotor hysteresis losses, $P_{\text{sh},0}$ and $P_{\text{rh},0}$, at the frequency f_0. Similarly, the term of the eddy current losses $P_{\text{e},0}$, which is the sum of the stator and rotor eddy current losses $P_{\text{se},0}$ and $P_{\text{re},0}$, is referred to f_0.

3) Stator Current Calculation: with the computed iron losses and current components ($i_{d\text{-}m}$, $i_{q\text{-}m}$, and i_r), the active and reactive powers at the terminal *aa'* in Fig. 1 can be calculated:

$$\begin{cases} P_{aa'} = \frac{3}{2} \cdot (i_{d-m} \cdot e_d + i_{q-m} \cdot e_q) + P_{Fe} \\ Q_{aa'} = \frac{3}{2} \cdot (i_{d-m} \cdot e_q - i_{q-m} \cdot e_d) \end{cases} \tag{8}$$

The stator current components $\mathbf{i}_{dq}$ are then derived as:

$$\begin{cases} i_d = \frac{2}{3} \cdot \frac{e_d \cdot P_{aa'} + e_q \cdot Q_{aa'}}{e_{dq}^2} \\ i_q = \frac{2}{3} \cdot \frac{e_q \cdot P_{aa'} - e_d \cdot Q_{aa'}}{e_{dq}^2} \end{cases} \tag{9}$$

4) Copper Losses Calculation: the stator and rotor copper losses are computed as:

$$P_{\text{Cu,s}} = \frac{3}{2} \cdot R_s \cdot i_{dq}^2, \quad P_{\text{Cu,r}} = R_r \cdot i_r^2 \tag{10}$$

where $i_{dq} = \sqrt{i_d^2 + i_q^2}$ represents the magnitude of the stator current vector $\mathbf{i}_{dq}$, and the resistances R_s and R_r are scaled according to the considered stator and rotor temperatures.

5) Electrical Active and Reactive Power Calculation: the total stator power is then calculated as:

$$P_e = P_{aa'} + P_{\text{Cu,s}}, \quad Q_e = Q_{aa'} \tag{11}$$

6) Voltage and Power Factor Computation: the stator voltages are determined as:

$$\begin{cases} v_d = \frac{2}{3} \cdot \frac{i_d \cdot P_e - i_q \cdot Q_e}{i_{dq}^2} \\ v_q = \frac{2}{3} \cdot \frac{i_q \cdot P_e + i_d \cdot Q_e}{i_{dq}^2} \end{cases} \tag{12}$$

The rotor voltage is computed as:

$$v_r = R_r \cdot i_r \tag{13}$$

Finally, the power factor is calculated using:

$$\cos\varphi = \cos\left(\arctan\left(\frac{v_q}{v_d}\right) - \arctan\left(\frac{i_q}{i_d}\right)\right) \tag{14}$$

7) Efficiency Computation: the mechanical power P_m is obtained as:

$$P_m = T_m \cdot \omega_m \tag{15}$$

The overall efficiency η is then evaluated as in (16),where P_l represents the total losses.

$$\eta = \frac{P_m}{P_m + P_l} \tag{16}$$

C. Feasibility Check and Control Strategies

Among all the combinations of $i_{d\text{-}m}$, $i_{q\text{-}m}$, and i_r currents that can produce the considered torque, some operating points must be ruled out to respect the source constraints as in (17), where V_{lim} is the maximum stator voltage, I_{lim} is the maximum stator current, and $I_{r,\text{lim}}$ is the maximum rotor current.

$$v_{dq} \leq V_{\text{lim}}, \quad i_{dq} \leq I_{\text{lim}}, \quad i_r \leq I_{r,\text{lim}} \tag{17}$$

Finally, among the feasible operative points, the algorithm selects the final combination of currents based on the considered control strategy. The procedure is then repeated for each torque and speed combination of the (T_m, n_m) plane.

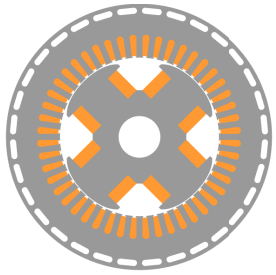

Fig. 3. The EESM case study cross-section.

TABLE I
THE EESM CASE STUDY RATINGS.

Machine Characteristics	
Number of pole pairs	2
Number of stator slots	48
Winding type	stranded
Type of cooling	air
Peak torque	245 Nm
Base speed	4000 rpm
Maximum speed	12000 rpm
Peak phase current	380 Apk*
DC-link voltage	400 V
Maximum excitation current	13 A*
Stator resistance @20°C	9.8 mΩ
Rotor resistance @20°C	5.7 Ω

**Estimated*

IV. COMPUTED EFFICIENCY MAPS

The proposed procedure has been applied to generate the efficiency maps of a 100kW electrically excited traction motor used in automotive applications, whose cross-section is depicted in Fig. 3, and its key specifications are listed in Table I. A detailed FE model has been used to generate the necessary flux and loss maps. The procedure has been applied assuming both the stator and rotor windings at the same temperature (i.e., $25°C$), although different thermal conditions can be easily analyzed using the same approach. Five distinct control strategy cases have been considered to demonstrate the procedure's adaptability in evaluating the impact of different control strategies on the machine's performance across the entire operating range.

Moreover, although the procedure does not account for AC copper losses and mechanical losses, the obtained results can still provide valuable insights into the behavior of EESMs. Indeed, in the considered case study (stranded windings with a wire diameter of approximately 0.8 mm and a maximum operative frequency of 400 Hz), the contribution of AC losses is expected to be negligible, as evidenced by [5], where a 1.2 mm wire at 400 Hz showed less than a 5% increase in the copper losses of the active sides of the conductors. Additionally, the impact of mechanical losses can be incorporated at a later stage by associating them with the mechanical load.

1) Minimize total losses P_l: this case represents the most common objective in electric machine efficiency mapping, as the overall efficiency is maximized. The resulting efficiency map is presented in Fig. 4. The map highlights a distinctive feature of EESMs: their ability to maintain high efficiencies

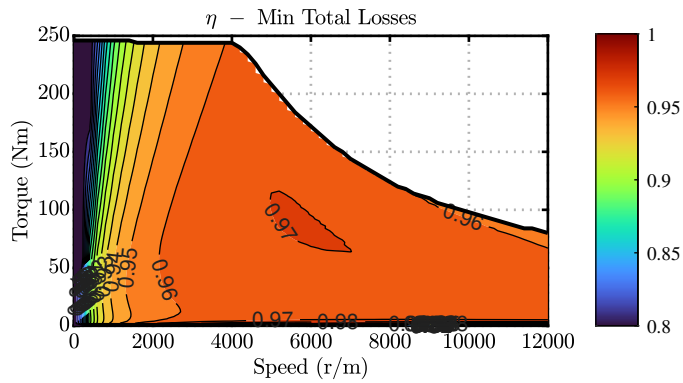

Fig. 4. Efficiency map for the minimum total losses strategy.

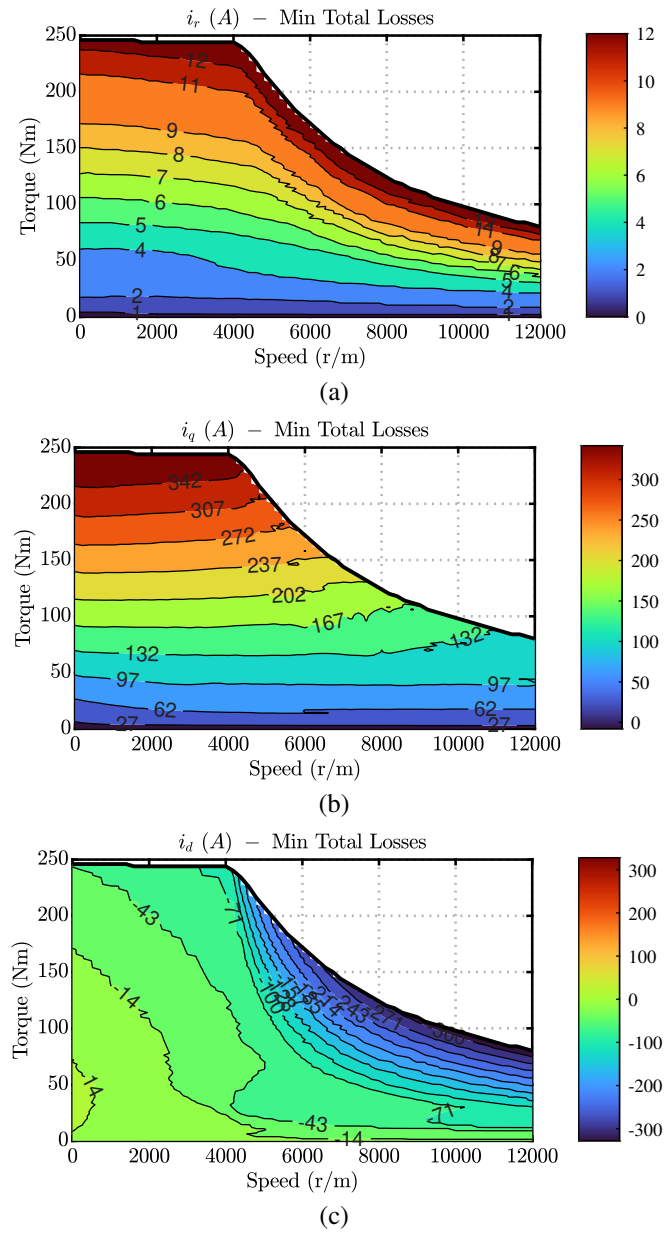

Fig. 5. Maps of the rotor and stator current components for the minimum total losses strategy.

across a wide range of operating points due to the possibility of adjusting the rotor current. A detailed analysis of the corresponding i_d, i_q, and i_r maps, shown in Fig. 5, reveals how the excitation current, i_r, is adjusted mainly on the basis of the torque demand, together with the q-axis current. Conversely, flux weakening is achieved by injecting progressively larger negative d-axis currents (i_d). This control strategy ensures optimal efficiency operation compared to the forthcoming cases, whose efficiency maps are shown in Fig. 6-9.

2) Minimize copper losses $P_{Cu,s}+P_{Cu,r}$: this strategy aims at minimizing only the copper losses in both the stator and rotor windings. Its key advantage lies in its practicality for implementation, as copper losses can be readily computed from the winding resistance values. However, the trade-off for this practical approach is evident in Fig. 6. Compared to the efficiency map shown in Fig. 4, the resulting map exhibits slightly lower efficiency values since only a part of the overall losses is minimized. The main difference is observed in the high-speed, low-torque region, where iron losses have a greater impact than copper losses. Despite this drawback, the compromise may be acceptable depending on the specific application requirements, as it simplifies the computational effort while still achieving reasonable efficiency levels.

3) Minimize rotor losses $P_{Cu,r} + P_{Fe,r}$: consists of minimizing only the rotor losses, including both iron and copper contributions. This approach helps mitigate rotor overheating, which is essential in applications with limited cooling capabilities. As illustrated in Fig. 7, the resulting efficiency map shows lower efficiency values compared to Fig. 4. This outcome is primarily due to the reduction of the rotor current compared to the levels shown in Fig. 5a, as depicted in Fig.10a. Indeed, this reduction is compensated not only by an increase in the q-axis current component to ensure the necessary torque level, as shown in Fig.10b, but also by an increase in the d-axis current to ensure sufficient machine magnetization. This adjustment leads to higher overall losses, ultimately resulting in lower efficiency, while offering the advantage of lowering losses in the inner part of the machine, where heat extraction is more challenging. Although this improves thermal management, determining the extent of its impact would require the development of a detailed thermal model of the motor. Such a model, which is outside the scope of this paper, would account for the resistance variations due to temperature changes.

4) Maximize power factor $\cos(\varphi)$: aims to minimize the machine's reactive power, which is a highly desirable characteristic for several reasons. A high power factor indicates that almost all of the machine's apparent power is converted into active power, comprising the output mechanical power and losses. Furthermore, a higher power factor improves inverter utilization, enabling more efficient operation. In the design stage, it can also allow for smaller and more cost-effective inverter sizes. As shown in Fig. 8, there are no significant differences compared to the efficiency map in Fig. 4, which confirms that EESM machines generally operate at high power factor levels. For a detailed comparison, the resulting power

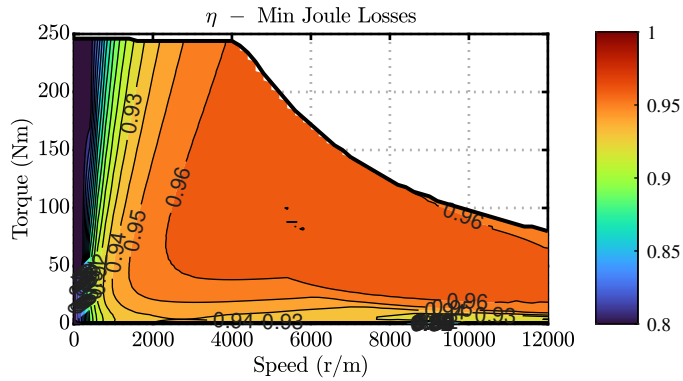

Fig. 6. Efficiency map for the minimum copper losses strategy.

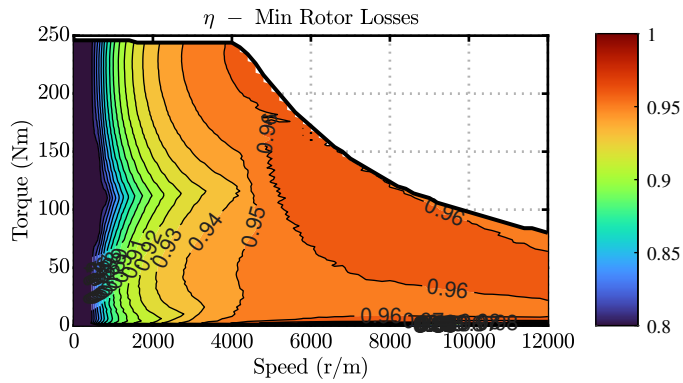

Fig. 7. Efficiency map for the minimum rotor losses strategy.

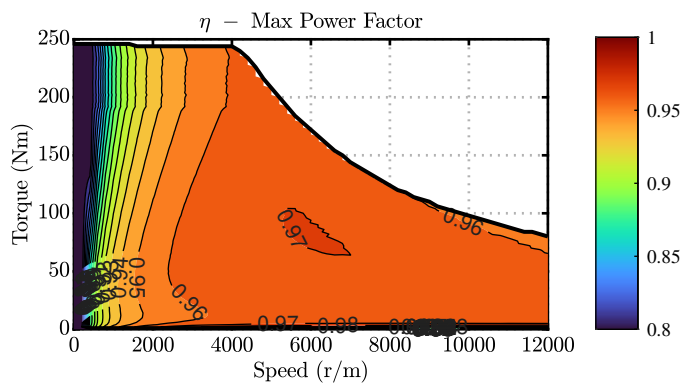

Fig. 8. Efficiency map for the maximum power factor strategy.

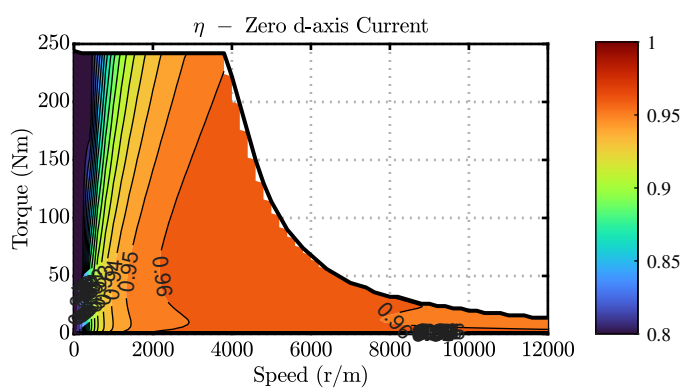

Fig. 9. Efficiency map for the zero d-axis current strategy.

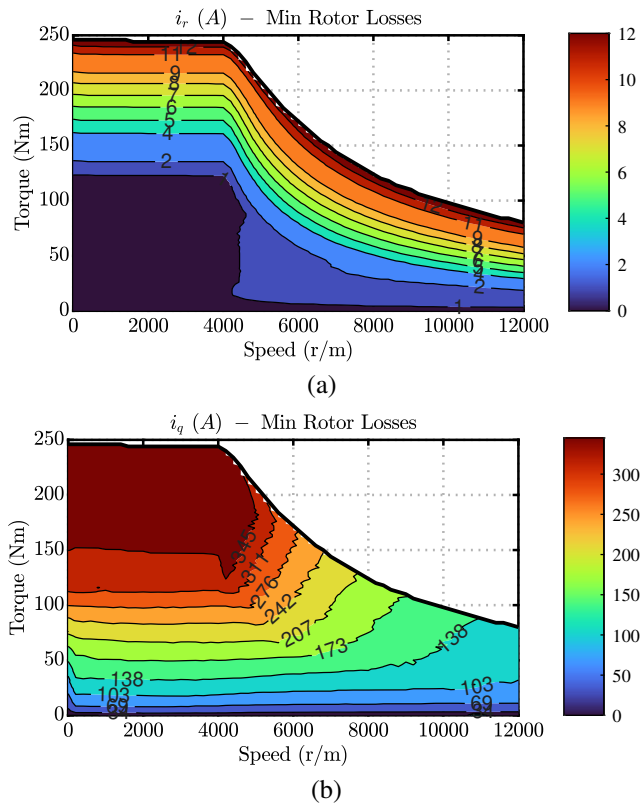

Fig. 10. Maps of the rotor and q-axis stator current components for the minimum rotor losses control strategy.

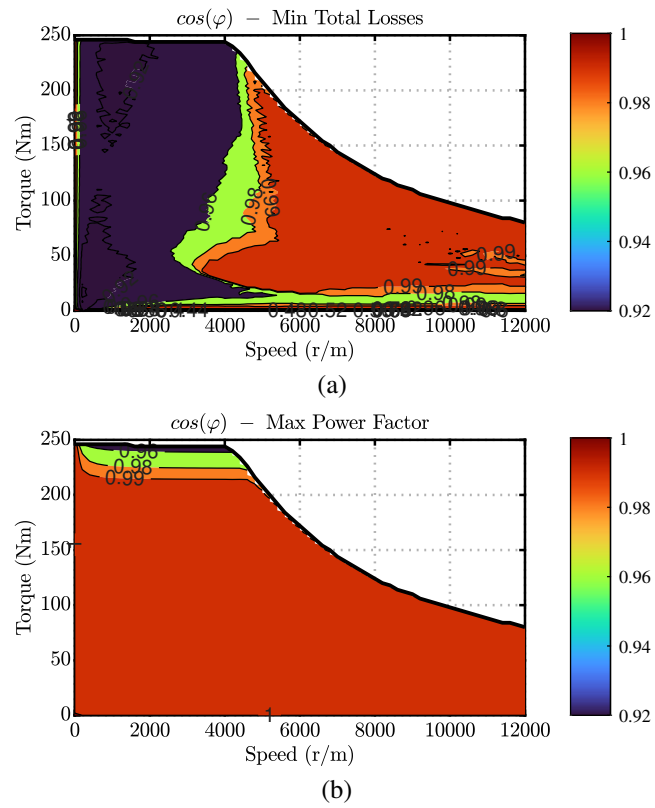

Fig. 11. Power factor map: for the minimum total losses strategy (a) and the maximum power factor strategy (b).

factor maps for case 1) and case 4) are presented in Fig. 11.

5) Zero d-axis current i_d: this case considers injecting current only along the q-axis, on the stator side. To achieve this, a null d-axis current is enforced in computing the efficiency maps under all operating conditions. This case aims to investigate the impact of the d-axis current in the field-weakening region. The results, which are consistent with those reported in [8], are shown in Fig. 9. The torque envelope decreases rapidly with increasing speed, confirming that the constant power speed range cannot be achieved solely by adjusting the rotor current, as previously evidenced by Fig. 5.

V. Conclusion

This paper presented an efficiency mapping procedure for electrically excited synchronous motors, offering a comprehensive methodology to evaluate their performance across the entire operating range. The proposed procedure is based on the machine flux and loss maps and is capable to optimize motor operation under different control strategies. The methodology was demonstrated using an electrically excited motor mounted on a commercial vehicle, considering five different control strategies: minimizing total losses, copper losses, or rotor losses, maximizing power factor, and maintaining null d-axis current. The procedure effectively generated the EESM efficiency maps under different conditions (e.g., inverter limits, winding temperatures) and readily adapted to the different control strategies, providing valuable insights into their impact on motor efficiency.

References

[1] Z. Ran, Z.-Q. Zhu, Z. Chen, M. Younkins, P. Farah, and J. Fuerst, "Drive-cycle system efficiency evaluation of electrically excited synchronous machine with dynamic motor drive," in *PEMD*, 2024.

[2] "Valeo and MAHLE expand their product range of magnet free electric motors to upper segment applications through a Joint Development of iBEE," accessed: 16-December-24. [Online]. Available: https://www.valeo.com/en/valeo-and-mahle-expand-their-product-range-of-magnet-free-electric-motors-to-upper-segment-applications-through-a-joint-development-of-ibee-inner-brushless-electrical-excitation/

[3] F. Filippini, M. Pastura, and N. Bianchi, "PM and PM-Less Motors for Electric Vehicles: A Comparative Analysis," in *ICEM*, 2024.

[4] F. Graffeo, S. Vaschetto, A. Tenconi, and A. Cavagnino, "Fast sizing procedure for salient-pole wound field synchronous motors for transportation electrification," in *IEEE IEMDC*, 2023, pp. 1–7.

[5] S. Ferrari, P. Ragazzo, G. Dilevrano, and G. Pellegrino, "Flux and loss map based evaluation of the efficiency map of synchronous machines," *IEEE Transactions on Industry Applications*, 2023.

[6] O. Stiscia, S. Rubino, S. Vaschetto, A. Cavagnino, and A. Tenconi, "Accurate induction machines efficiency mapping computed by standard test parameters," *IEEE Transactions on Industry Applications*, vol. 58, no. 3, pp. 3522–3532, 2022.

[7] J. O. Estima and A. J. Marques Cardoso, "Efficiency analysis of drive train topologies applied to electric/hybrid vehicles," *IEEE Transactions on Vehicular Technology*, 2012.

[8] W. Q. Chu, Z. Q. Zhu, J. Zhang, X. Liu, D. A. Stone, and M. P. Foster, "Investigation on operational envelops and efficiency maps of electrically excited machines for electrical vehicle applications," *IEEE Transactions on Magnetics*, 2015.

[9] S. Müller and N. Parspour, "Applying a measurement-based iron loss model to an efficiency optimized torque control of an electrically excited synchronous machine," in *ICEM*, 2020.

[10] E. Armando, R. I. Bojoi, P. Guglielmi, G. Pellegrino, and M. Pastorelli, "Experimental identification of the magnetic model of synchronous machines," *IEEE Transactions on Industry Applications*, vol. 49, no. 5, pp. 2116–2125, 2013.